

Experimental and numerical studies on seismic performance of hollow RC bridge columns

Qiang Han^{*1,2}, Yulong Zhou^{1,2}, Xiuli Du^{1,2}, Chao Huang³ and George C. Lee³

¹Key Laboratory of Urban Security and Disaster Engineering of Ministry of Education, Beijing University of Technology, Beijing 100124, China

²Beijing Collaborative Innovation Center for Metropolitan Transportation, Beijing 100124, China

³MCEER, University at Buffalo, The State University of New York, Buffalo, NY 14260, U.S.A

(Received December 6, 2014, Revised February 11, 2014, Accepted April 23, 2014)

Abstract. To investigate the seismic performance and to obtain quantitative parameters for the requirement of performance-based bridge seismic design approach, 12 reinforced concrete (RC) hollow rectangular bridge column specimens were tested under constant axial load and cyclic bending. Parametric study is carried out on axial load ratio, aspect ratio, longitudinal reinforcement ratio and transverse reinforcement ratio. The damage states of these column specimens were related to engineering limit states to determine the quantitative criteria of performance-based bridge seismic design. The hysteretic behavior of bridge column specimens was simulated based on the fiber model in OpenSees program and the results of the force-displacement hysteretic curves were well agreed with the experimental results. The damage states of residual cracking, cover spalling, and core crushing could be well related to engineering limit states, such as longitudinal tensile strains of reinforcement or compressive strains of concrete, etc. using cumulative probability curves. The ductility coefficient varying from 3.71 to 8.29, and the equivalent viscous damping ratio varying from 0.19 to 0.31 could meet the requirements of seismic design.

Keywords: bridge columns; hollow section; cyclic load; damage state; seismic performance

1. Introduction

Hollow cross section is an optimized section type for bridge columns, which not only make effective use of the sectional properties but also reduce the mass contributions of bridge columns to the seismic response. Therefore, bridge columns with hollow section are widely used in bridge engineering, especially high and large span bridges in the high seismic intensity region of Western China. As shown in Fig. 1(a), a Chinese design code, Guideline for Seismic Design of Highway Bridges (JTG/T 2008) provides a detailed configuration of hollow rectangular section for reinforced concrete (RC) columns, which is based on the advised configuration by Priestley, et al. (1996). Though this section provides good seismic performance for bridge columns, a lot of stirrup and transverse bracing reinforcements are needed, thus it is costly and inconvenient to install. In order to maintain satisfactory ductility and to facilitate constructability, a different configuration of

*Corresponding author, Associate Professor, Ph.D., E-mail: qhan@bjut.edu.cn

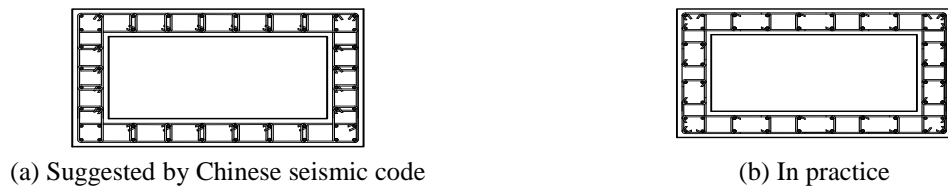


Fig. 1 Configuration of transverse reinforcement of hollow rectangular cross section

transverse reinforcement in practice as shown in Fig. 1(b) is proposed. However, many concerns of structural behaviors and design parameters need to be studied for this configuration of transverse reinforcement, including: the seismic performance of hollow rectangular RC bridge column, the design methodology of the construction measure to satisfy the displacement requirement of columns, the parametric study on the seismic performance and the modeling parameters for performance-based design, and the development of nonlinear analytical models for such columns subjected to strong earthquake excitation, etc.

In the past few decades, researchers carried out a lot of studies about hollow RC bridge columns subjected to the axial load and uniaxial bending, and developed some numerical models to analyze the seismic nonlinear responses. Several analytical models, which can predict the seismic performance of RC bridge columns, were presented by Kent *et al.* (1971), Park *et al.* (1985), Priestley *et al.* (1987, 1996), Hoshikuma *et al.* (1997) and Mander *et al.* (1998). But all the above were carried out based on the experimental results of solid RC bridge columns. Calvi *et al.* (2005) proposed an analytical model and a reinforcement measure by studying insufficient shear capacity and lacking of transverse constrains for hollow RC circle bridge columns. Yeh *et al.* (2001, 2002), Mo *et al.* (2004) and Pinto *et al.* (2003) studied the seismic performance of hollow RC square bridge columns and provided the seismic response with prediction models according to their different country seismic design codes. Cheng *et al.* (2003) and Mo *et al.* (2004) studied the seismic performance of hollow RC bridge columns with FRP reinforcement. However, the section types and reinforcement configurations of hollow columns are significantly different from RC solid columns. There is still a lack of information on hollow RC rectangular bridge columns subjected to strong seismic excitation in China.

The main objectives of this paper are: 1) to evaluate seismic performance and damage patterns of hollow RC rectangular bridge columns subjected to a constant axial load and cyclic uniaxial bending by experiments of 12 1/4 scale specimens, and 2) to provide quantitative parameters for performance-based bridge seismic design and connect structural damage states with engineering limit states.

2. Experimental program

2.1 Overview

A series of experiments were designed to obtain the seismic performance for hollow RC rectangular bridge columns. Based on a hollow RC rectangular bridge column in practice, the sectional dimension of each column specimen was a 1/4 scaled actual column. Cross sections of the prototype and the specimen were 2.0×1.5 m and 0.5×0.36 m, respectively. The wall thickness of

Table 1 Properties of bridge column specimens

Specimen	Height (mm)	Aspect ratio	Axial load (MN)	Axial load ratio	Longitudinal reinforcement		Transverse reinforcement		
					Diameter (mm)	ρ_l	Diameter (mm)	Spacing (mm)	ρ_s
S1	1440	4	0.28	0.1	40D8	0.014	D4/6	40	0.035
S2	1440	4	0.28	0.1	40D10	0.021	D4/6	40	0.035
S3	2880	8	0.28	0.1	40D8	0.014	D4/6	40	0.035
S4	2880	8	0.28	0.1	40D10	0.021	D4/6	40	0.035
S5	2880	8	0.56	0.2	40D8	0.014	D4/6	40	0.035
S6	2880	8	0.56	0.2	40D10	0.021	D4/6	40	0.035
S7	2880	8	0.28	0.1	40D10	0.021	D4/6	55	0.025
S8	3600	10	0.28	0.1	40D8	0.014	D4/6	40	0.035
S9	3600	10	0.28	0.1	40D10	0.021	D4/6	40	0.035
S10	3600	10	0.56	0.2	40D8	0.014	D4/6	40	0.035
S11	3600	10	0.56	0.2	40D10	0.021	D4/6	40	0.035
S12	3600	10	0.28	0.1	40D10	0.021	D4/6	55	0.025

the prototype and the specimen was 400 mm and 120 mm, respectively. Fig. 2(a) shows the configuration of columns and reinforcement.

Table 1 lists the properties of 12 specimens, including axial load ratio, aspect ratio, longitudinal reinforcement ratio and transverse reinforcement ratio. The 12 specimens were divided into four test groups. The first test group studied effect of varying axial load ratios, including S3 and S5, S4 and S6, S8 and S10, S9 and S11. The varying parameter for the second test group is the aspect ratio, including S1, S3 and S8, as well as S2, S4 and S9. The third test groups examined effect of varying longitudinal reinforcement ratios, including S1 and S2, S3 and S4, S5 and S6, S8 and S9, S10 and S11. The varying parameter for the last group is the transverse reinforcement ratio, including S4 and S7, S9 and S12.

2.2 Reinforcement design

The longitudinal reinforcement ratio of bridge columns varies with the criteria and recommendations of design codes from different countries. In China, the range of rational longitudinal reinforcement ratio is from 0.6% to 4.0%. However, the value is between 1.0% and 8.0% in the United States and between 0.8% and 8.0% in New Zealand. The minimum longitudinal reinforcement ratio of 0.5% is permitted in Japan. In this series of experiments, the longitudinal reinforcement ratio of specimens is 1.4% or 2.1%, which is reasonable and economical, and also meets the requirements of Chinese seismic design code.

The design of the transverse reinforcement is compliant with the requirements of concrete core confinement and shear resistance in JTG/T (2008) as well as the requirements of AASHTO (2007) and Priestley, *et al.* (1996). In this study, all the specimens can meet the requirements except the specimens S7 and S12. Therefore it is necessary to enhance the transverse confinement in potential plastic hinge regions for S7 and S12. The lengths of potential plastic hinge, L_p , of Caltrans (2006), AASHTO (2007) and JTG/T B02-01 (2008) are obtained from Eqs. (1), (2), and (3), respectively.

$$L_p \geq \max (1.5b_b, l_1, 0.25l_2) \tag{1}$$

$$L_p \geq \max (b_{max}, 1/6h_0, 457\text{mm}) \tag{2}$$

$$L_p \geq \max (b_{max}, 1/6h_0, 500\text{mm}) \tag{3}$$

where b_b is the cross sectional dimension in the direction of bending, l_1 is the length of the region where the moment exceeds 75% of the maximum plastic moment, l_2 is the distance from the point of maximum moment to the inflexion point, b_{max} is the maximum dimension of cross section, and h_0 is the height of the column.

2.3 Material properties

The same reinforcement and concrete materials used in the prototype column were used for all the specimens, resulting in the stress scaling factor to be 1.0. HRB335 (a Chinese steel grade) was used for the reinforcement with a design yielding strength of 300MPa. The longitudinal bars were

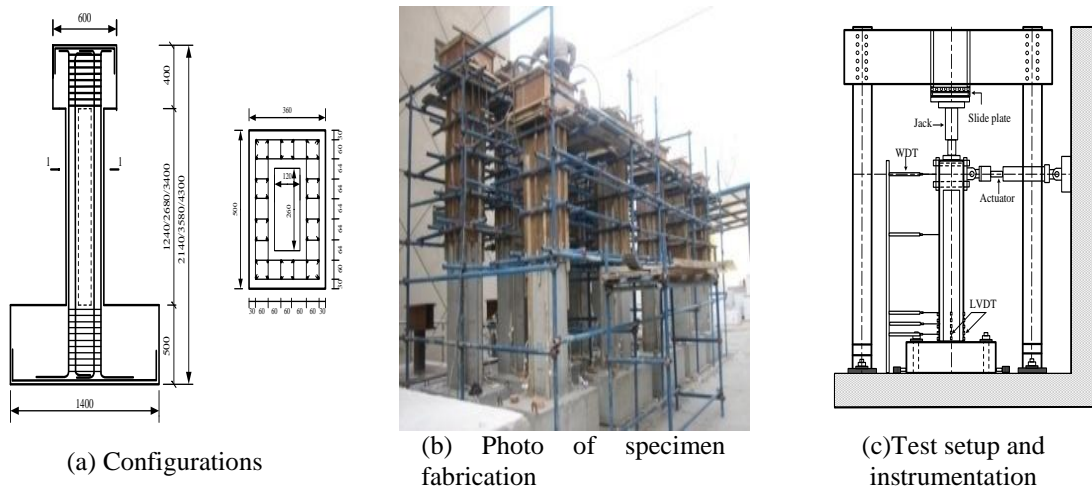


Fig. 2 Specimen and test setup



Fig. 3 Photo of column experiment

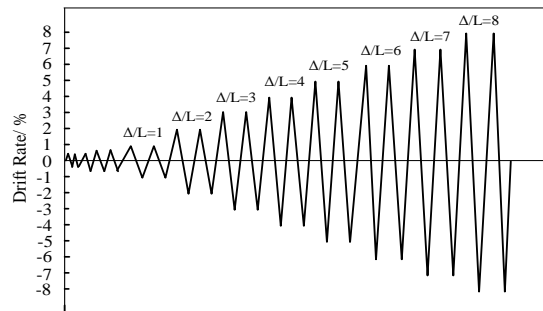


Fig. 4 Displacement history

8 mm or 10 mm in diameter, and the transverse bars were 6 mm in diameter. C40 (a Chinese concrete grade) was used for the concrete with a design compressive strength of 19.1MPa. The average measured values of the yielding strength and ultimate strength from standard tensile coupon tests were 392MPa and 498MPa, respectively. The average measured compressive strength of concrete was 41.3MPa, which was obtained by $150 \times 150 \times 150$ mm concrete cubic tests after 28-day curing process. Both the reinforcement and concrete strength measured were higher than the design strength.

2.4 Test setup and instrumentations

Fig. 2(b) shows a photo of specimen fabrication in the laboratory. The column specimens were fabricated and tested at the Key Laboratory of Urban Security and Disaster Engineering of Beijing University of Technology, China. The specimens were instrumented to monitor global responses (e.g., applied lateral load and displacement) as well as local responses (e.g., steel strains and column segment strains). The same test setup and instrumentations were used for all 12 specimens, as depicted in Fig. 2(c). The instrumentations for local responses were distributed in the plastic hinge region and extended to a certain distance above it. Along the length of columns, external instrumentations were used to monitor lateral deformation, and local segment expansion of the specimens. Foil strain gauges on the longitudinal and transverse reinforcement were installed to monitor the strains within the footing and above the footing.

2.5 Loading protocol

Fig. 3 shows a typical test setup, in which the specimen was mounted vertically on a strong base and bended by both lateral loading and constant axial loading applied on the top. The constant axial load is $0.1A_gf_c'$ or $0.2A_gf_c'$, where A_g is the gross cross sectional area of columns and f_c' is the concrete compressive design strength. Based on different drift or displacement requirements for columns with different heights, two cycles were applied at each level of the lateral displacement history. Experimental data were collected automatically by electronic instruments. The loading protocol was shown in Fig. 4. The concrete crack and spalling, reinforcement yield and fracture, etc., were observed and recorded during the loading process.

3. Observed damage states and engineering limit states

Three stages of structural performance levels, including usage state, damage state and structure stability state, can be connected to the structural properties of stiffness, strength and ductility. Fig. 5 shows the typical performance curve of structures. It is difficult to design a column that satisfies all the demands of stiffness and strength if more intermediate performance levels were considered (Moehle 2004). The implementation of performance-based seismic design needs to determine the quantitative damage states and reasonable reinforcement measures, which can be accomplished by the engineering limit states that represented by values of peak strains or cyclic damage indices, etc. as illustrated in Fig. 6 (Ghobarah 2001).

Table 2 shows that structural damage states are the bridges between engineering limit states and performance levels. Hence, the key issue in the performance-based seismic design is to obtain

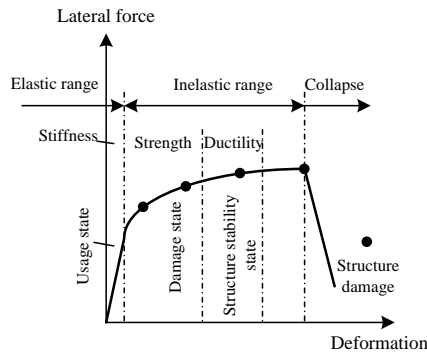


Fig. 5 Typical performance curve of structures

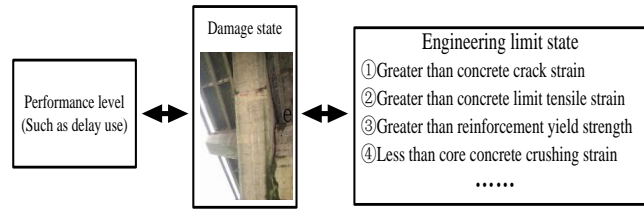


Fig. 6 Relation between performance level, damage state and engineering limit state

Table 2 Relationship of engineering limit states and performance levels

□ Check limit states		Engineering limit state				
		Concrete crazing	Concrete spalling	Residual drift rate	Reinforcement fatigue	Sectional failure
Levels of performance	Normal use	<input checked="" type="checkbox"/>	<input type="checkbox"/>	<input type="checkbox"/>	<input type="checkbox"/>	<input type="checkbox"/>
	Delay use	<input checked="" type="checkbox"/>	<input checked="" type="checkbox"/>	<input type="checkbox"/>	<input type="checkbox"/>	<input type="checkbox"/>
	Structure stability	<input checked="" type="checkbox"/>	<input checked="" type="checkbox"/>	<input checked="" type="checkbox"/>	<input checked="" type="checkbox"/>	<input type="checkbox"/>

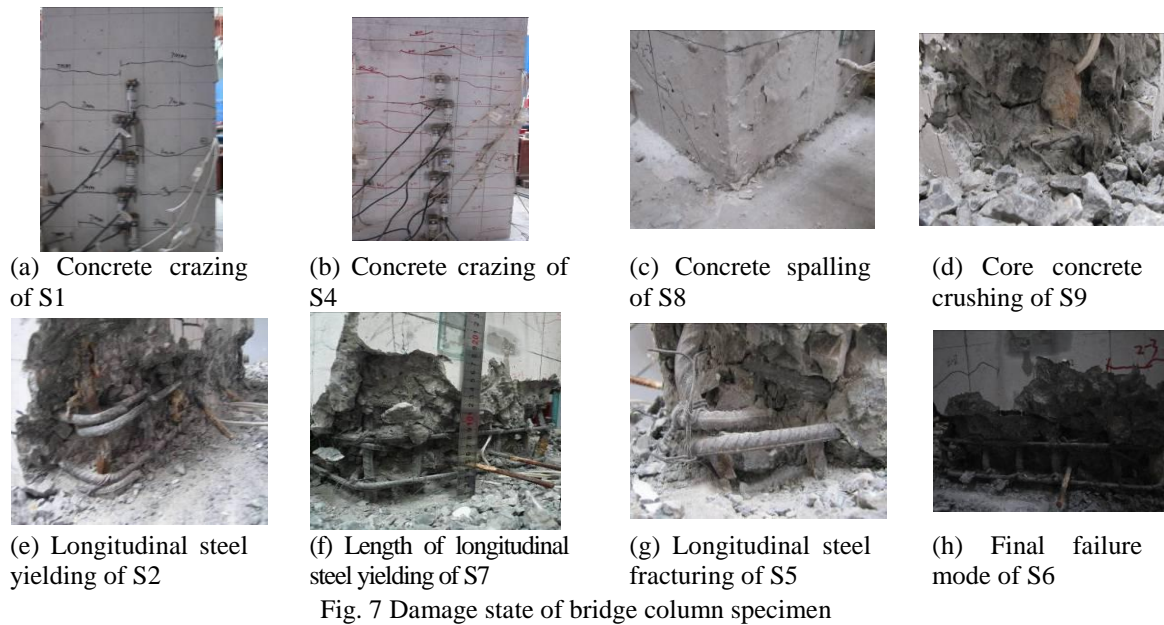


Fig. 7 Damage state of bridge column specimen

quantified damage states through establishing the connection between measured damage states in practice and engineering limit states.

Table 3 Damage parameters of bridge columns

Specimen	Initial yielding displacement (mm)	Concrete cover initial spalling			Concrete core initial crushing		Spalling region	
		Horizontal displacement (mm)	Height (mm)	Compressive strain	Horizontal displacement (mm)	Compressive strain	Height (mm)	Spalling height/Column height (%)
S1	13.11	32	76	-0.0076	62	-0.016	119	8
S2	13.08	32	72	-0.0097	64	-0.014	143	10
S3	20.71	57	108	-0.0042	102	-0.011	317	11
S4	21.98	59	110	-0.0039	98	-0.024	376	13
S5	19.64	57	86	-0.0054	96	-0.016	402	14
S6	21.36	57	89	-0.0048	102	-0.031	458	16
S7	18.06	58	85	-0.0081	102	-0.019	395	14
S8	20.10	71	124	-0.0042	121	-0.021	324	9
S9	20.37	72	132	-0.0053	127	-0.014	193	11
S10	19.74	71	114	-0.0037	114	-0.019	472	13
S11	20.29	71	122	-0.0053	119	-0.023	546	15
S12	20.07	72	97	-0.0029	128	-0.018	467	13

The sequences of damage were similar for all columns. In sequence of occurrence, they were: concrete cracking, longitudinal reinforcement yielding, concrete cover spalling, concrete core crushing, hooping fracture, longitudinal reinforcement buckling, and longitudinal reinforcement fracture. These damage states are described in Figs. 7(a-h). Table 3 gives the detailed damage parameters of bridge columns in the test.

3.1 Cracking and yielding

When the lateral displacement reached 3 mm, the initial damage occurred in terms of horizontal cracks with an initial spacing of approximately 15 mm, which equals to half of the cross sectional dimension in the bending direction (Fig. 7(a)). With increasing levels of displacement, new cracks appeared and the spacing of cracks decreased (Fig. 7(b)). With further increasing displacement, bending cracks developed and finally distributed in the region with the height of approximately 500 mm from the footing.

Initial yielding of the longitudinal reinforcement was obtained by a strain gauge which was attached to the extreme longitudinal reinforcement above the interface of the column and footing. The measured initial yield displacement for each specimen, u_y , is listed in Table 4.

The occurrence of concrete cracking has an important influence on the stiffness of the column. The identification of open residual cracks is a challenge of performance-based seismic design, as it may be used to determine which method should be applied for the retrofit technology of bridge piers. Some design codes link the crack width with the maximum strain of longitudinal reinforcement. For example, ATC-32 (1996) suggests that the residual strain is related to the maximum strain directly, while ACI 318 (2008) recommends that the maximum crack width is related to the maximum strain indirectly. China design code (JTG 2004) has no regulation, but it limits the crack width in different types of sites, e.g., the maximum crack width is limited to 0.2 mm in the sites I and II, and value is limited to 0.15 mm in the sites III and IV.

The residual crack width, w_{res} , was recorded when the displacement was zero after two cycles of loading. For the specimens with the aspect ratio (ratio of height to width) of 4, the residual crack width was measured at the height of 100 mm and 200 mm from the footing interface, while

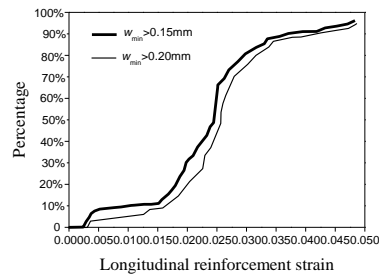


Fig. 8 Cumulative probability curves for different residual crack widths

for those with the aspect ratio of 8 and 10, the residual crack width was measured at the height of 200 mm and 300 mm, respectively. The stress of the longitudinal reinforcement in the outermost layer was obtained by the strain gauges that was attached on the reinforcement in the specimens. The deterministic relationship of the measured stress and residual crack width cannot be established because of the insufficient and discrete data obtained from the test. However, the relationship can be illustrated by cumulative probability curves of residual crack width. Fig. 8 shows the cumulative probability curves with residual crack width exceeding 0.15mm and 0.20mm, where the x -coordinate represents maximum strain of longitudinal reinforcement in the outermost layer and the y -coordinate represents the percentage of residual crack width beyond 0.15mm or 0.20mm.

3.2 Spalling and crushing

The occurrence and development of concrete spalling are significant parameters to evaluate the performance for bridge columns. Following yielding of the longitudinal reinforcement, initial spalling of the concrete cover will occur above the footing interface of columns, as shown in Fig. 7(c). With the development of the concrete spalling, the damage of the concrete core will occur. The spalling length along the height of columns is also an important parameter which decides the minimum height of transverse reinforcements from the footing interface. To improve the seismic performance of bridge columns, it is necessary to select an effective method for repairing the spalling and crushing of concrete.

The strain of the initial spalling of concrete covers ranges widely from -0.0029 to -0.0097, with a mean of -0.0054, a standard deviation of 0.0021 and a coefficient of variation of 0.39. ATC-32 (1996) suggests the value of compression strain of outermost concrete spalling is -0.004, which equals to the mean value minus two thirds of standard deviation in terms of experimental data. Fig. 9(a) and Fig. 9(b) present the distributed and cumulative probability curves corresponding to compressive strain of concrete spalling and crushing, respectively.

Note that the initial spalling did not occur at the interface between the column and footing, instead at a distance, h_{spall} , above the interface. Fig. 10(a) shows the relation between spalling strain ε_{spall} and the corresponding spalling height h_{spall} , which is that ε_{spall} increase with the decreasing of h_{spall} . One reason of this variation may be that the concrete close to the base is confined by the footing. Another reason may be that the ε_{spall} is influenced by the moment gradient along the height of the column. For columns with small aspect ratios, the moment gradients is usually steep, thus the sections with higher strain demand can be confined by adjacent sections



Fig. 9 Distributed and cumulative probability curves for compressive strain



Fig. 10 Relation of initial spalling strain with spalling height and aspect ratio

with lower strain demand, as shown in Fig. 10(b). Therefore, the columns with higher moment gradients tended to have larger initial spalling strains. Other parameters such as stirrup reinforcement ratio and longitudinal reinforcement ratio had no significant influence on the spalling strain.

The main damages of concrete cover and core, which are difficult to be directly measured by external instrumentation, resulted from larger displacement levels and manifold cycles. Hence, the damage of concrete core can be only evaluated through observations. In the test process, the damage state was defined based on the displacement level at which the inside transverse reinforcement was fully exposed (see Fig. 7(d)). Table 3 lists the strains and other damage parameters corresponding to initial crushing of the concrete core. Other parameters such as the axial load ratio, aspect ratio, longitudinal reinforcement ratio or transverse reinforcement ratio etc., have no obvious relationship with damage states.

3.3 Buckling, fracture, and loss of lateral load-carrying capacity

In general, once the concrete cover had completely spalled off as well as the longitudinal and transverse reinforcement were exposed, the buckling of longitudinal reinforcement was observed within the next displacement cycle (Fig. 7(e)). In all cases, the buckled portion of the reinforcement spanned several hoops. The lateral displacement of the buckled reinforcement increased during subsequent displacement cycles at a given displacement level. The fracture of transverse reinforcement was resulted from excessive lateral deformation of the buckled bar. For all columns, the length of the buckled region was similar, i.e., approximately 6% of the column height above the base (Fig. 7(f)). Fracture of the longitudinal reinforcement occurred after reinforcement buckling (Fig. 7(g)). However, reinforcement fracture was only observed for part of

the columns. Fig. 7(h) shows the final state of the specimen S6.

Cyclic history has a more prominent influence on reinforcement buckling than on damage to concrete, such as spalling. In general, failure is initiated by buckling of longitudinal reinforcement, so compressive strain is recommended as the key parameter in this paper. Nevertheless, the maximum tension strain may be more important due to the Bauschinger effect, the instantaneous tangent modulus and compressive stress under cyclic loading are controlled by the stroke of tension strain. Therefore, the peak strains are insufficient for the characterization of the failure of columns subjected to generalized loads.

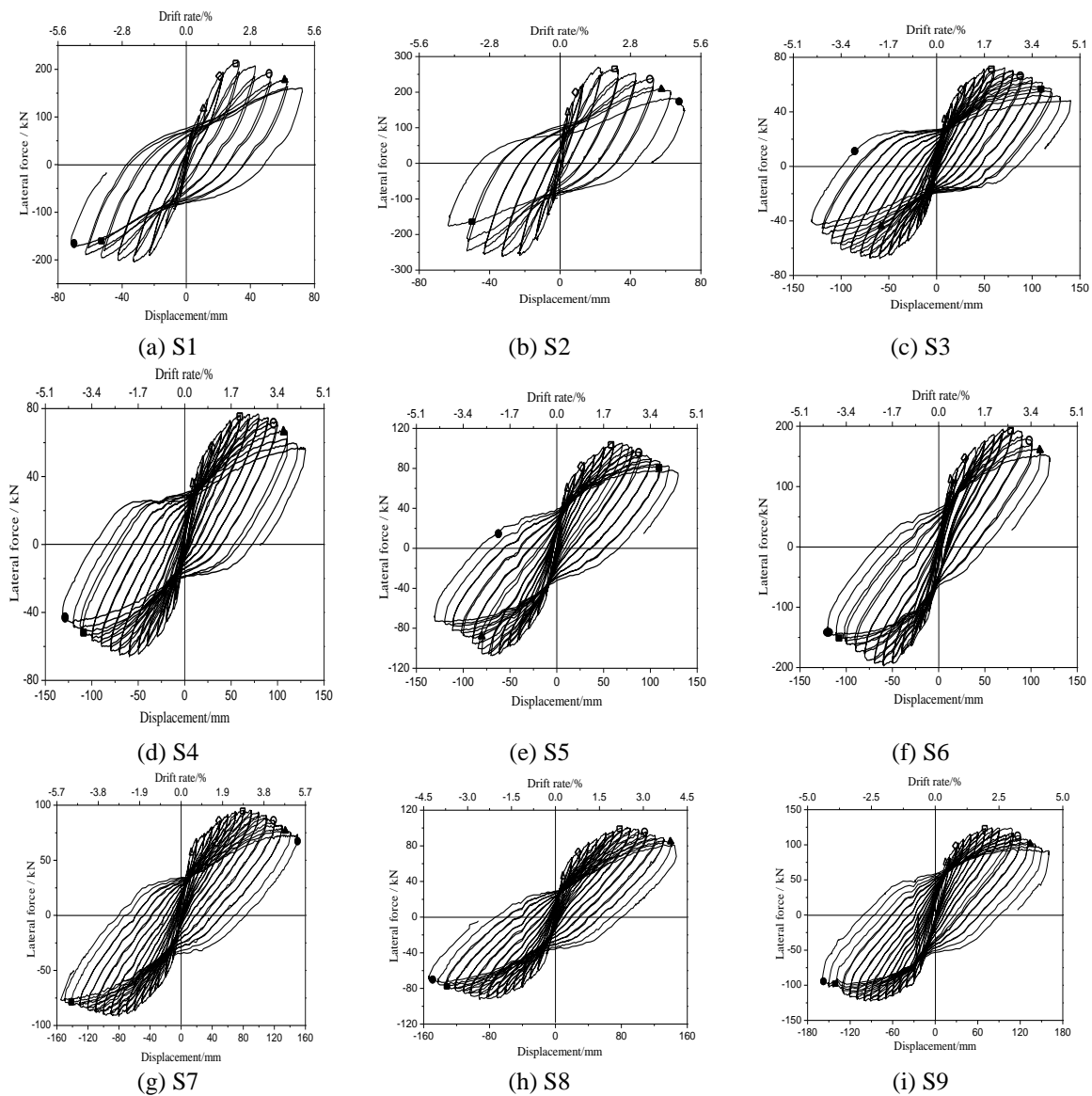


Fig. 11 Continued

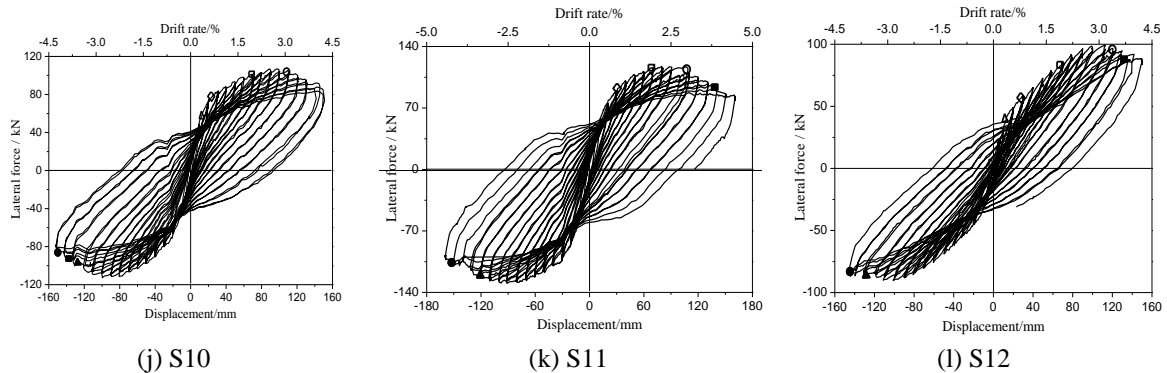


Fig. 11 Load-Displacement Hysteretic Curves of Specimens

4. Experimental results and analysis

4.1 Lateral load-displacement hysteretic response and envelop curves

Fig. 11 shows the lateral load-displacement hysteretic loops. Several characteristics are summarized as follows: (1) before the yielding of longitudinal reinforcement, the area enclosed by each single hysteretic loop is small, and the loading and unloading stiffness of columns does not degrade, (2) after the yielding of longitudinal reinforcement, inelastic deformation appears and the loading and unloading stiffness of columns gradually degrades. Degradation of stiffness accelerates with the increasing of test cycle count. The hysteretic loops are plump and the enclosed areas increase. The pinching phenomenon is not distinct, which means the columns with such transverse reinforcement have good seismic performance, and (3) after reaching maximum loading, the area of hysteretic loops become larger and the shape of hysteretic loops is plumper. Due to the increase of deformation, the yielding range of the column extends. The stiffness of columns deteriorates gradually as the deformation increase. The stiffness of unloading and initial loading remains almost the same, but pinching phenomena are evident.

To qualitatively evaluate the seismic performance of specimens such as strength, ductility, etc., skeleton curves of 12 specimens were taken by connecting peak points of each single lateral load-displacement hysteretic loop, as shown in Fig. 12. The skeleton curves show that: 1) with the increase of the longitudinal reinforcement ratio, the lateral bearing capacity improves and the extent of descending branch decreases, especially for the specimens with large axial load ratios, the increasing effect on the capacity is dramatic, 2) with the increase of the transverse reinforcement spacing, the capacity of specimens declines slightly, which concludes that the transverse reinforcement spacing has slight effect on the capacity, and 3) The columns with the axial load ratio of 0.2 have larger stiffness in elastic and strengthening stages and longer hardening stage than those with the axial load ratio of 0.1. With the loading displacement continually increasing, the yielding of the longitudinal reinforcement and the spalling of the concrete cover results in the drop of load-displacement hysteretic curves. With larger axial load ratio, the drop of hysteretic curves is larger. From the viewpoint of lateral bearing capacity, the axial load ratio of 0.2 is a more reasonable option for bridge design than 0.1.

4.2 Ductility capacity

The ductility capacity is defined as the inelastic deformability in the case of little initial strength degenerating. The ductility capacity reflects the structural energy dissipation capability and deformability. The ductility factor μ can be expressed by Eq. (4), namely the ratio of the ultimate displacement u_u to the yield displacement u_y ,

$$\mu = \frac{u_u}{u_y} \quad (4)$$

The yield displacement is defined as the displacement corresponding to the initial yield of a longitudinal reinforcement. Strain gauge measurements indicate that the longitudinal reinforcements at the corners yielded first, which are highlighted in Fig. 7(e). The ultimate displacement is defined as the displacement corresponding to the 85% of the maximum lateral force in the descending stage.

Table 4 gives the result for the measured values of displacement and ductility ratio. It can be seen that: 1) with the increase of the longitudinal reinforcement ratio, the ductility factor declines. The short columns decline in a more extent of 25%, which is induced by the larger stiffness of short columns, 2) with the increase of the transverse reinforcement spacing, the ductility factor increases obviously, which is not accordant with general performance of reinforced concrete members. The reason may attribute to the larger stiffness caused by larger amount of transverse reinforcements, so a smaller ratio of transverse reinforcements results in better ductility capacity, and 3) the fact that ductility factors decline distinctly when the axial load ratio increases from 0.1 to 0.2, which proves that the axial load ratio has significant effect on the ductility capacity of columns.

Overall, ductility factors of specimens range from 3.71 to 8.29. These ductility factors over 3.0 reflect that the specimens provide good ductility, plastic deformation capacity and collapse-resist performance.

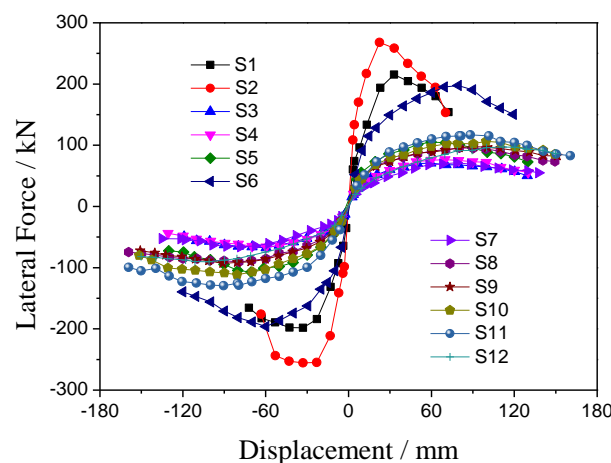


Fig. 12 Envelop curves of specimens

Table 4 Measured values of displacement and ductility ratio

Specimen	Cracking u_{cr} / mm	Yielding u_y / mm	Max load u_d / mm	Limit load u_u / mm	Ductility factor μ_u
S1	3.97	13.11	33.02	64.93	4.95
S2	4.13	13.08	22.75	48.57	3.71
S3	10.25	20.71	59.59	113.17	5.46
S4	11.85	21.98	71.76	117.41	5.34
S5	9.75	19.64	65.16	98.12	5.00
S6	9.96	21.36	69.70	104.07	4.87
S7	8.01	18.06	78.28	128.31	7.10
S8	10.07	20.10	90.79	132.51	6.59
S9	10.28	20.37	90.16	130.06	6.38
S10	10.97	19.74	87.73	128.60	6.51
S11	11.63	20.29	85.29	116.72	5.75
S12	9.89	20.07	100.45	166.31	8.29

4.3 Strength and stiffness degradation

The strength degradation is defined as the lateral load capacity decreases with the increasing count of test cycles. It can be expressed by the loading degradation factor λ_i which is regarded as an index of general degradation behavior in the loading and unloading processes. The loading degradation factor is defined as the ratio of the peak loading in the one specific cycle, P_i , to the maximum loading value of specimen column, P_{max} , namely, $\lambda_i = P_i/P_{max}$. The strength degradation curves of 12 column specimens are shown in Figure 13. Two lines represent $\lambda_i = 0.8$ and $\lambda_i = -0.8$ correspond to the limit lateral loading capacity ($P_u = 0.80P_{max}$). It can be seen from that this type of columns has a long enough horizontal plateau after yielding, i.e., the lateral capacity will remain in a high level, so the columns can bear the load after reaching the maximum load. Fig. 13 also shows the influence of different parameters on the strength degradation coefficient.

The phenomenon that the stiffness of columns decreases with the increase of loading-displacement is defined as stiffness degradation. Fig. 14 shows the curves of stiffness-lateral displacement of 12 specimens. The stiffness decreases with the increase of displacement, and the curves become more and more gentle. The reason is that the development of concrete cracks results in the cracking concrete stop working, which decreases the effective cross section property gradually.

4.4 Energy dissipation

The dissipated energy in one hysteresis loop, ΔW_i , is determined by calculating the area enclosed by the hysteresis loop as indicated by Eq. (5). The accumulative energy dissipated in the column specimens is the area enclosed by all hysteresis loops. $F_l(u)$ and $F_{ul}(u)$ are the force functions of displacement u during loading and unloading processes.

$$\Delta W_i = \int_{-u_{min}}^{u_{max}} (F_l(u) - F_{ul}(u)) du \tag{5}$$

Equivalent damping ratio, ζ_{eq} , an index of energy dissipation capacity, can be calculated by Eq. (6), namely the ratio of the dissipated energy in one cycle, to the strain energy of an equivalent linear elastic system.

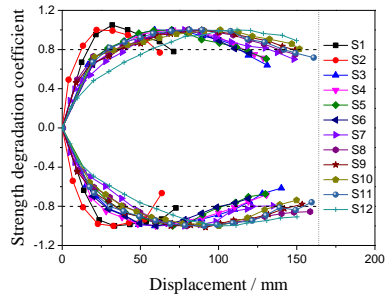


Fig. 13 Strength degradation curves of specimens

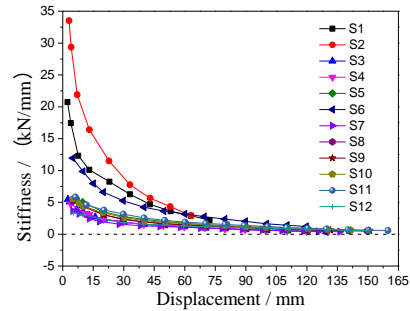


Fig. 14 Stiffness degradation curves of specimens

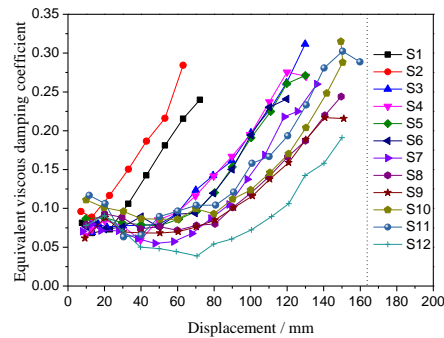


Fig. 15 Equivalent damping ratio of specimens

$$\xi_{eq} = \Delta W_i / (2\pi k u_{max}^2) \quad (6)$$

Where k is the secant stiffness and u_{max} is the maximum displacement in a cycle. Fig. 15 presents the equivalent damping of strong and weak axes versus drift for 12 specimens. The maximum equivalent damping ratios of specimens vary from 0.19 to 0.31, which are slightly larger than those of general RC solid section columns. Therefore, energy dissipation of hollow rectangular cross-section RC columns with the lateral reinforcement configuration is good, and the index of energy dissipation meets the specified seismic design requirement of concrete structures in China.

5. Numerical method based on OpenSees platform

5.1 Model of element

This paper employs Beam with Hinges Element from the nonlinear beam element library in OpenSees to simulate bridge columns, as shown in Fig. 16. This element is proposed by Scott, *et al.* (2006) based on the flexibility formulation and considering plasticity to be concentrated over specified hinge lengths at the two element ends. A reasonable hinge length of L_p at the bottom and a hinge length of 0 at the top is placed. The middle region of element keeps linear elastic behavior

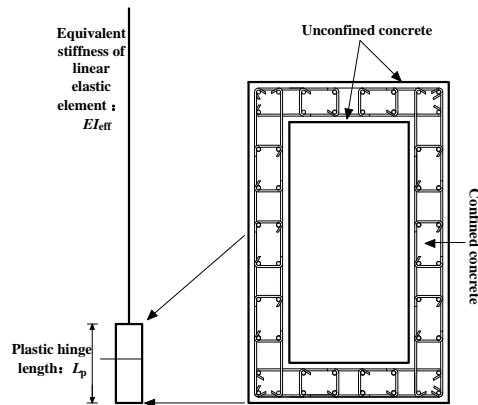


Fig. 16 Beam with hinges element

all along. Therefore, the setting of an accurate hinge length is important to achieve better computational accuracy and efficiency.

In this test, plastic hinge length is obtained by an equation proposed by Priestly, *et al.* (1996), which can be expressed by Eq. (7):

$$L_p = 0.08L + 0.022f_y d_s \geq 0.044f_y d_s \quad (7)$$

where L is the height of columns, f_y is the yielding strength of longitudinal reinforcement and d_s is the diameter of longitudinal reinforcement.

To consider the influence of bond-slip on hysteretic characteristics, Zero-Length Section Element is placed at the bottom of column in numerical models, which divides the deformation into two parts: bending effect simulated by a nonlinear element and bond-slip effect simulated independently by a zero-length element.

5.2 Constitutive of material

For RC columns, transverse stirrups with reasonable configurations and sufficient amounts can provide appropriate constraint to concrete core, which not only increase the compressive strength and compressive strain limit, but also affect the descending branches for concrete core. Hence it is important to choose a reasonable constitutive model to simulate the concrete behavior mentioned above. In this study, both the confined and unconfined concrete employ Concrete 01 from the material library in OpenSees which is proposed by Scott *et al.* (1982) and the stress-strain relation is shown in Fig. 17(a).

Under the cyclic loading, the constitutive relation of reinforcement has significant effect on the result of hysteretic characteristics. Therefore, an appropriate and reasonable stress-strain relation ensures the validity of numerical model. This paper selects Reinforcing Steel from the material library in OpenSees which is proposed by Chang and Mander (1994). This reinforcement model can take main hysteretic characteristics of reinforcement into account, e.g., isotropic strain hardening, initial yielding plateau, Bauschinger effect, buckling, strength degradation, stiffness degradation and rupture. Fig. 17(b) shows the stress-strain relation of Mander-Chang reinforcement model.



Fig. 17 Constitutive relation of material

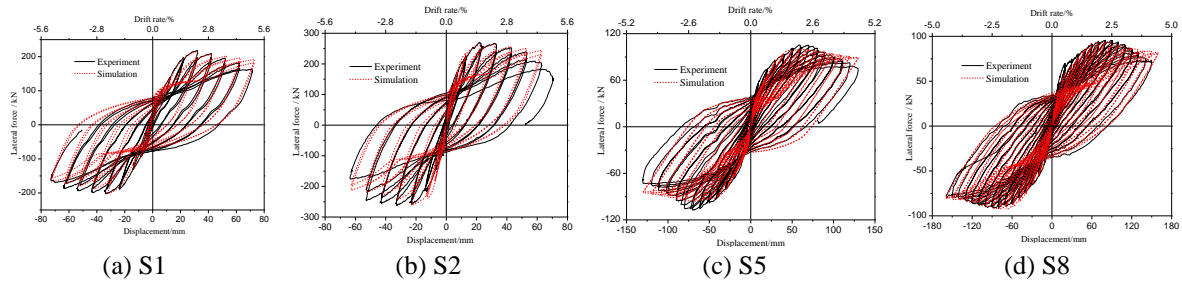


Fig. 18 Comparison of simulated and experiment hysteretic curves

To consider the strength and stiffness degradation caused by cyclic loading, Coffin-Mason model (Brown, Kunnath 2000) is introduced into the reinforcement model. In Coffin-Mason model, there are three parameters α , C_f and C_d , which control the fatigue and rupture of reinforcement. Recommended values for three parameters are 0.506, 0.26 and 0.389 proposed by Brown and Kunnath (2000) from low cycle fatigue tests. In addition, Berry (2007) provided that the three reference values are 0.506, 0.26 and 0.45 through numerical analysis. In this paper, these three parameters are obtained through actual material characteristic test as well as considering the reference values mentioned above.

6. Numerical results and compared with experiment

The results of numerical simulation by OpenSees were compared with the hysteretic curves obtained from the experiments. Fig. 18 shows the on the hysteretic curves for four typical columns, and Table 5 shows the comparison on the characteristic values of experiments and numerical results. It can be seen that there is a 10%~ 20% deviations in terms of yield load between the simulation and experiment results, because numerical method cannot accurately consider the stiffness degradation caused by concrete cracking. However, the maximum load has merely a deviation below 10%. Except for S1 and S2, all specimens have a deviation of ultimate load less than 6%.

The comparisons indicate that the simulated results show good agreement with those from experiments. It can be concluded that for hollow RC rectangular columns under cyclic loading, the fiber model considering the bond-slip influence together with Concrete 01 model and Reinforcing Steel model could well simulate the hysteretic characters such as the strength and stiffness

Table 5 Comparison of characteristics of skeleton curves

Specimen	Yielding load (kN)			Maximum load (kN)			Ultimate load (kN)		
	Test	Simulation	Deviation (%)	Test	Simulation	Deviation (%)	Test	Simulation	Deviation (%)
S1	132.38	136.51	3.1	206.66	216.34	4.7	175.66	199.41	13.5
S2	214.28	175.78	-18.0	261.49	266.63	2.0	222.26	249.33	12.2
S3	46.89	53.41	13.9	69.53	70.98	2.1	59.10	60.41	2.2
S4	48.76	57.76	18.5	71.76	72.71	1.3	61.00	62.11	1.8
S5	69.69	62.88	-9.8	106.19	100.35	-5.5	90.26	87.34	-3.2
S6	131.78	113.13	-14.2	196.82	181.41	-7.8	167.30	157.52	-5.8
S7	35.78	30.21	-15.6	68.67	63.99	-6.8	58.37	59.36	1.6
S8	61.30	53.56	-12.6	93.09	90.49	-2.8	79.13	83.56	5.6
S9	61.55	49.41	-19.7	94.50	92.51	-2.1	80.33	84.73	5.5
S10	66.78	59.87	-10.3	110.45	108.69	-1.6	93.88	91.82	-2.2
S11	76.65	61.44	-19.8	123.20	120.62	-2.1	104.72	103.14	-1.5
S12	45.63	40.65	-10.9	93.23	91.85	-1.5	79.25	76.92	-2.9

degradation, load and unload processes, pinch effect, etc.

However, there is a distinct difference about 15% between the result from simulation and experiment in terms of descending branches, because the strong nonlinearity caused by the strength and stiffness degradation could not be accurately simulated based on the fiber model and the plane cross-section assumption. Therefore, it is necessary to carry out the study of descending branches for RC hollow bridge columns. The numerical results are slightly greater than those of the experimental for specimens with small aspect ratio, because the shear effect which has much greater effect on short-medium columns is not considered.

7. Conclusions

12 hollow RC bridge column specimens with rectangular cross section were tested under constant axial load and cyclical bending to investigate their seismic performance. Parametric study was carried out on the axial load ratio, aspect ratio, longitudinal reinforcement ratio and lateral reinforcement ratio. The hysteretic behavior of bridge column specimens was simulated using the fiber model. The obtained numerical results were then compared to the experimental results. The following conclusions can be drawn:

(a) The experimental results showed that the ductility coefficient varied from 3.71 to 8.29 and the equivalent viscous damping ratio varied from 0.19 to 0.31, which meet all the requirements of Chinese seismic design code. The hollow rectangular RC bridge columns with the configurations of lateral reinforcement studied in this paper not only provide good seismic performance, but also reduce the quantities of transverse bars and make the construction more convenient compared to the configuration given in current Chinese bridge seismic design code.

(b) Based on the tests results, cumulative probability curves for different residual crack widths, distributed and cumulative probability curves for compressive strain during concrete cracking and

spalling, as well as the relations of initial spalling strain and spalling height, initial spalling strain and aspect ratio were obtained. Also, structural damage states were related to engineering limit states in order to obtain the quantitative indices for performance-based seismic design.

(c) The Beam with Hinges Element and Zero-Length Section Element using the fiber model were able to accurately simulate strength and stiffness degradation, loading and unloading processes, pinching phenomena, *etc.*, of hollow rectangular RC columns based on the OpenSees platform.

Acknowledgments

This research is jointly funded by the National Natural Science Fund of China (NSFC) (Grants No.51178008, No.51421005), the National Program on Key Basic Research Project (Grant No.2011CB013600) and the research project of Beijing Municipal Commission of Education (Grant KZ201410005011). This study is also a joint research project between the Beijing University of Technology and the University at Buffalo with partial support from the U.S. Federal Highway Administration (Contract No. DTFH61-07-C-00020). Their supports are gratefully acknowledged. The results and conclusions presented in the paper are of authors' and do not necessarily reflect the view of the sponsors.

References

- AASHTO (2007), *LRFD bridge design specifications*, American Association of State Highway and Transportation Officials, Washington (DC), USA.
- ACI (2008), *ACI 318-08 Building code requirements for structural concrete and commentary*, ACI Committee Institute, Farmington Hills, USA.
- ATC (1996), *ATC-32 Improved seismic design criteria for California bridges: provisional recommendations*, Applied Technology Council, California, USA.
- Berry, M.P (2007), "Performance modeling strategies for modern reinforced concrete bridge columns", *Pacific Earthquake Engineering Research Center*, University of California Berkeley, USA.
- Brown, J. and Kunnath, S.K. (2000), *Low Cycle Fatigue Behavior of Longitudinal Reinforcement in Reinforced Concrete Bridge Columns*, NCEER Technical Report 00-0007.
- CALTRANS (2006), *Bridge design specifications*, Sacramento California Department of Transportation, California, USA.
- Calvi, G.M., Pavese, A., Rasulo, A. and Bolognini, D. (2005), "Experimental and numerical studies on the seismic response of RC hollow bridge piers", *Bull. Earthq. Eng.*, **3**(3), 267-297.
- Chang, G. and Mander, J. (1994), *Seismic Energy Based Fatigue Damage Analysis of Bridge Columns: Part I-Evaluation of Seismic Capacity*, NCEER Technical Report 94-0006.
- Cheng, C.T., Yang, J.C., Yeh, Y.K. and Chen, S.E. (2003), "Seismic performance of repaired hollow-bridge piers", *Construct.Build. Mater.*, **17**(5), 339-351.
- Ghobarah, A. (2001), "Performance-based design in earthquake engineering: state of development", *Eng. Struct.*, **23**, 878-884.
- JTG (2004), *JTG D62-2004 Code for design of highway reinforced concrete and prestressed concrete bridges and culverts*, Ministry of Transport of the People's Republic of China, Beijing, China.
- JTG (2008), *JTG/T B02-01-2008 Guideline for seismic design of highway bridges*, Ministry of Transport of the People's Republic of China, Beijing, China.
- Hoshikuma, J., Kawashima, K., Nagaya, K. and Taylor, A.W. (1997), "Stress-strain model for confined

- reinforced concrete in bridge piers”, *J. Struct. Eng.*, **123**(5), 624-633.
- Kent, D.C. and Park, R. (1971), “Flexural member with confined concrete”, *J. Struct. Div.*, **97**(7), 1969-1990.
- Mander, J.B., Priestley, M.J.N. and Park, R. (1998), “Theoretical stress-strain model for confined concrete”, *J. Struct. Eng.*, **114**(8), 1804-1849.
- Mo, Y.L., Yeh, Y.K. and Hsieh, D.M. (2004), “Seismic retrofit of hollow rectangular bridge columns”, *J. Compos. Construct.*, **8**(1), 43-51.
- Mo, Y.L. and Nien, I.C. (2002), “Seismic performance of hollow high-strength concrete bridge columns”, *J. Bridge Eng.*, **7**(6), 338-349.
- Moehle, M.S., Calderone, A. and Henry, L. (2004), “Experimental evaluation of the seismic performance of reinforced concrete bridge columns”, *J. Struct. Eng.*, **130**, 869-879.
- Pinto, A.V., Molina, J. and Tsionis, G. (2003), “Cyclic tests on large-scale models of existing bridge piers with rectangular hollow cross-section”, *Earthq. Eng. Struct. Dyn.*, **32**(13), 1995-2012.
- Park, Y.J. and Ang, A.H.S. (1985), “Mechanistic seismic damage model for reinforced concrete”, *ASCE J. Struct. Eng.*, **5**(3), 722-739.
- Priestley, M.J.N., Seible, F. and Calvi, G.M. (1996), *Seismic Design and Retrofit of Bridges*, John Wiley & Sons, New York, NY, USA.
- Priestley, M.J.N. and Park, R. (1987), “Strength and ductility of concrete bridge columns under seismic loading”, *ACI Struct. J.*, **84**(1), 61-75.
- Priestly, M.J.N. and Benzoni, G. (1996), “Seismic performance of circular columns with low longitudinal reinforcement ratios”, *ACI Struct. J.*, **93**(4), 474-485.
- Scott, M.H. and Fenves, G.L. (2006), “Plastic hinge integration methods for force-based beam-column elements”, *J. Struct. Eng.*, **132**(2), 244-252.
- Scott, B.D., Park, R. and Priestly, M.J.N. (1982), “Stress-strain behavior of concrete confined by overlapping hoops at low and high strain rates”, *ACI J.*, **79**(1), 13-27.
- Yeh, Y.K., Mo, Y.L. and Yang, C.Y. (2001), “Seismic performance of hollow circular bridge piers”, *ACI Struct. J.*, **98**(6), 862-871.
- Yeh, Y.K., Mo, Y.L. and Yang, C.Y. (2002), “Seismic performance of rectangular hollow bridge columns”, *J. Struct. Eng.*, **128**(1), 60-68.
- Yeh, Y.K.; Mo, Y.L. and Yang, C.Y. (2002), “Full-scale tests on rectangular hollow bridge piers”, *Mater. Struct.*, **35**(2), 117-125.